Chlorination Chemistry 4. Ab Initio Study of the Addition, Metathesis, and Isomerization Channels Governing the Reaction of Chlorine Atom with Propargyl Chloride

Jeffrey W. Hudgens*,† and Carlos Gonzalez*,‡

Physical and Chemical Properties Division, Chemical Science and Technology Laboratory, National Institute of Standards and Technology, Gaithersburg, Maryland 20899

Received: October 22, 2001; In Final Form: March 19, 2002

Highly correlated ab initio molecular orbital calculations have been used to map out the potential energy surface corresponding to the reaction of Cl + propargyl chloride (C_3H_3Cl) in the gas phase. Ten transition state structures governing the mechanism of the title reaction were computed at seven different levels of theory up to QCISD(T)/6-311+G(d,p)//QCISD(T)/6-31+G(d,p). Chlorine atom additions at the center and end unsaturated carbons are barrierless processes forming incipient, chemically activated 2,3-dichloro-1-propen-1-yl and 1,3-dichloro-1-propen-2-yl radicals, respectively. The incipient radicals cannot isomerize by transferring a hydrogen atom because the governing transition state structures reside at ≥ 95 kJ·mol^{-1} above the initial reactants. The presence of a transition state for chlorine atom transfer below the energy of the initial reactants enables isomerization between the incipient radicals. A second accessible chlorine transfer transition state enables the 1,3-dichloro-1-propen-2-yl radical to isomerize into the more stable 1,2-dichloroallyl radical. The chemically activated 1,3-dichloro-1-propen-2-yl radical also undergoes bond scission of the chlorine atom in the chloromethyl group forming chloroallene and Cl atom. Chlorine atom attack on the chloromethyl group encounters metathesis transition states for HCl and Cl_2 formation at 5 kJ·mol^{-1} and 124 kJ·mol^{-1} above the initial reactants, respectively. The accord demonstrated between master equation calculations, based on the ab initio results, and experimental data validate the proposed reaction mechanism and predict that the dominant products of chlorine atom addition to propagryl chloride are chloroallene and the 1,2-dichloroallyl radical at 298 K and HCl, chloropropargyl radical, and chloroallene at 1000 K.

Introduction

Although the reactions of chlorine atoms with unsaturated hydrocarbons have roles during commercial syntheses and industrial waste incineration,[1] few rate coefficients are available for use in the computational modeling of these processes.[2] A contributing factor to this dearth of kinetic data may be the general apprehension that rate coefficient measurements for the larger alkynes and allenes are intractable due to the potential for many isomer products. Because isomers usually exhibit similar optical and mass spectra, temporally resolved species-specific measurements needed for accurate kinetic determinations become unfeasible. The design and interpretation of experimental kinetics studies of the larger unsaturated hydrocarbons are facilitated by knowledge of the governing elementary reaction mechanism. In recent years, ab initio calculations have become an efficient way for determining the most likely elementary reaction steps. In a preceding paper, we compared the transition state relative energies obtained at seven levels of ab initio theory for the Cl + allene reaction mechanism.[3] We found evidence that reliable energetics are obtained by using structure calculations at the QCISD, B3LYP, and MP2 levels followed by single point QCISD(T)/6-311+G(d,p) energy calculations that better captured the correlation energy. In this study, we report a similar ab initio study of the governing transition state structures for the very complex reaction, Cl + propargyl chloride. Master equation calculations, based on the ab initio results, are shown to be in accord with the available experimental data.

The Cl + propargyl chloride (3-chloropropyne, $CH_2ClC{\equiv}CH$) reaction exhibits the problems typical of reactions with unsaturated molecules containing three or more carbons. The thermochemistry of Cl + propargyl chloride allows for six exothermic product channels forming up to eleven distinct C3 isomers. Although gas-chromatographic analysis of the end products of Cl + propargyl chloride found only three chlorinated species, evidencing inactivity along some product channels, the end-product data is insufficient for ascertaining the reaction mechanism.[4,5] The uncertainty persists because two (or more) distinct radical products can undergo secondary reactions to produce the same species. For example, the 2,3-dichloro-1-propene end-product from the Cl + propargyl chloride reaction was easily identified by gas chromatography; however, this product may evidence production of either 1,2-dichloroallyl radical or 2,3-dichloro-1-propen-1-yl radical, or both species.[4]

An assignment of the Cl + propargyl chloride reaction mechanism is required for accurate rate determinations of the propargyl radical ($\cdot CH_2C{\equiv}CH$) recombination reaction rate coefficient, $k(C_3H_3 + C_3H_3)$. The ambient temperature experiments used to determine $k(C_3H_3 + C_3H_3)$ have initiated the reaction by photolyzing propargyl chloride with 193 nm light.[5−7] This method produces propargyl radicals in 93% yield[6]

$$C_3H_3Cl + 193\ nm \rightarrow \cdot C_3H_3 + \cdot Cl \quad (1a)$$

$$\rightarrow C_3H_2 + HCl \quad (1b)$$

At ambient temperature the photolytic chlorine atom population,

† E-mail: jeffrey.hudgens@nist.gov.
‡ E-mail: carlos.gonzalez@nist.gov.

10.1021/jp013920s CCC: $22.00
Published on Web 06/04/2002

TABLE 1: Ab Initio Results and Thermochemical Data Used to Estimate Relative Energies of the Persistent Species Involved in the Cl + Propargyl Chloride System

species	$\Delta_f H_0^{o\,a}$ kJ·mol^{-1}	$\Delta_f H_{298.15}^{o\,a}$ kJ·mol^{-1}	ref
Cl	119.62 ± 0.01	121.30 ± 0.01	45
Cl_2	0.0	0.0	45
Chloroallene	179 ± 6	173 ± 6	4
Chloropropargyl radical	316 ± 8	315 ± 8	4
3-chloro-propynyl radical ($CH_2ClC{\equiv}C\cdot$)	498 ± 7	495 ± 7	4
(*E*)−1,2-dichloroallyl radical	117 ± 6	110 ± 6	4
(*Z*)−1,2-dichloroallyl radical	121 ± 6	114 ± 6	4
(*E*,*Z*)−1,3-dichloroallyl radical	112 ± 6	105 ± 6	4
(*E*)−1,3-dichloro-1-propen-2-yl radical	228 ± 4	221 ± 4	4
(*Z*)−1,3-dichloro-1-propen-2-yl radical	228 ± 4	221 ± 4	4
2,3-dichloro-1-propen-1-yl radical	230 ± 4	223 ± 4	4
HCl	−92.1 ± 0.4	−92.3 ± 0.4	45
Propargyl chloride	185 ± 4	180 ± 4	4
Propargyl radical	341 ± 8	339 ± 8	46

[a] Indicated error is two standard deviations (2σ) propagated from the underlying measurements and does not include systematic error of the calculations.

which is equal to the C_3H_3 population, mainly adds to propargyl chloride forming a substantial chlorinated C3 radical ensemble. As observed in previous kinetic and spectroscopic studies,[5,8] cross-reactions between the C_3H_3 radical and chlorinated radical ensembles accelerate the depletion of the C_3H_3 concentration. Extraction of $k(C_3H_3 + C_3H_3)$ from such experiments must use a computational kinetic model that accounts for the recombination and cross-rate reactions among the isomers and C_3H_3. The most important feature of the adopted kinetic model is the number of different, highly reactive products predicted for the Cl + propargyl chloride reaction at 298 K; that is, does the reaction of Cl + propargyl chloride give one, or more than one, free radical species? In our previous experimental study, we adopted a kinetic model that presumed that Cl + propargyl chloride generated only one persistent free radical species. Using this model and knowledge of $k(C_3H_3Cl + C_3H_3Cl)$, we showed that the transient absorption kinetic data observed, whereas monitoring C_3H_3 and C_3H_3Cl concentrations gave consistent determinations of $k(C_3H_3 + C_3H_3)$ and $k(C_3H_3 + C_3H_3Cl)$.[5,8]

The kinetic model used in our previously reported experimental determinations was based upon a preliminary set of ab initio molecular orbital calculations of the mechanisms governing the Cl + propargyl chloride reaction. This report describes these ab initio molecular orbital calculations fully. We derive the governing mechanism of Cl + propargyl chloride and we show that this mechanism is consistent with the experimental kinetic rate data and end-product data reported previously.[5,8] The present ab initio results enable estimates of the high pressure and temperature rate coefficients of Cl + propargyl chloride by use of master rate equation methods.[9−12]

Elementary Reaction Channels of Cl + Propargyl Chloride. The reaction of Cl with propargyl chloride may proceed through metathesis or through chlorine addition channels. The metathesis reactions are

$$CH_2Cl\text{-}C{\equiv}CH + \cdot Cl \rightarrow CH_2Cl\text{-}C{\equiv}C\cdot + HCl$$
$$\Delta_{rxn}H^o_{298.15} = +(102 \pm 8)\ \text{kJ·mol}^{-1} \quad (2)$$

$$\rightarrow \cdot CHClC{\equiv}CH + HCl$$
$$\Delta_{rxn}H^o_{298.15} = -(78 \pm 8)\ \text{kJ·mol}^{-1} \quad (3)$$

$$\rightarrow \cdot CH_2C{\equiv}CH + Cl_2$$
$$\Delta_{rxn}H^o_{298.15} = +(39 \pm 8)\ \text{kJ·mol}^{-1} \quad (4)$$

where the enthalpies of reaction are calculated using the thermochemical data listed in Table 1 and the indicated uncertainty is two standard deviations (2σ). Chlorine addition may produce an incipient, chemically activated $C_3H_3Cl_2$ radical ensemble comprised of two, distinct vinylic isomers

$$CH_2Cl^{\gamma}{-}C{\equiv}CH + \cdot Cl^{\beta} \rightleftarrows CH_2Cl^{\gamma}{-}CCl^{\beta} = \dot{C}H$$
$$\Delta_{rxn}H^o_{298.15} = -(78 \pm 6)\ \text{kJ·mol}^{-1} \quad (5)$$

$$\rightleftarrows CH_2Cl^{\gamma}{-}\dot{C} = CHCl^{\beta}$$
$$\Delta_{rxn}H^o_{298.15} = -(79 \pm 6)\ \text{kJ·mol}^{-1} \quad (6)$$

The Greek letter annotations distinguish between the incumbent and reacting chlorine atoms. Chlorine addition to the center carbon forms the chemically activated 2,3-dichloro-1-propen-1-yl radical (reaction **5**). Chlorine addition to the unsaturated end carbon forms chemically activated 1,3-dichloro-1-propen-2-yl radical (reaction **6**). At 298 K and 625 Pa (~4.7 Torr) the combined rate of reactions 5 and 6 is $k(Cl + C_3H_3Cl) = k_5 + k_6 = (1.2 \pm 0.2) \times 10^{-10}$ cm^3·molecule^{-1}·s^{-1}, which is approaching the gas-kinetic limit.[8] Because both incipient $C_3H_3Cl_2$ adducts contain ~−(79 ± 6) kJ·mol^{-1} of chemical activation, these chemically activated species may also undergo further unimolecular reactions, including reverse reactions −**5** and −**6**, until collisionally stabilized. By transferring a chlorine atom, the chemically activated 2,3-dichloro-1-propen-1-yl radical may isomerize forming 1,3-dichloro-1-propen-2-yl radical

$$CH_2Cl^{\gamma}{-}CCl^{\beta}{=}\dot{C}H \underset{1,2\text{-Cl}}{\overset{2,1\text{-Cl}}{\rightleftarrows}} CH_2Cl^{\gamma}{-}\dot{C} = CHCl^{\beta}$$
$$\Delta_{rxn}H^o_{298.15} = -(1 \pm 4)\ \text{kJ·mol}^{-1} \quad (7)$$

The incipient, chemically activated 2,3-dichloro-1-propen-1-yl radical may isomerize forming 1,2-dichloroallyl radical by transferring a chlorine atom

$$CH_2Cl^{\gamma}{-}CCl^{\beta} = \dot{C}\,H \xrightarrow{3,1\text{-Cl}} \cdot[CH_2{\cdots}CCl^{\beta}{\cdots}CHCl^{\gamma}]$$
$$\Delta_{rxn}H^o_{298.15} = -(78 \pm 6)\ \text{kJ·mol}^{-1} \quad (8)$$

or by transferring a hydrogen atom

$$CH_2Cl^{\gamma}{-}CCl^{\beta} = \dot{C}\,H \xrightarrow{3,1\text{-H}} \cdot[CHCl^{\gamma}{\cdots}CCl^{\beta}{\cdots}CH_2]$$
$$\Delta_{rxn}H^o_{298.15} = -(78 \pm 6)\ \text{kJ·mol}^{-1} \quad (9)$$

Besides reverse reaction −**7**, three other channels may deplete the 1,3-dichloro-1-propen-2-yl radical population. The 1,3-dichloro-1-propen-2-yl radical may isomerize to 1,2-dichloroallyl radical through chlorine transfer

$$CH_2Cl^{\gamma}-\dot{C}=CHCl^{\beta} \xrightarrow{3,2\text{-Cl}} \cdot[CH_2\cdots CCl^{\gamma}\cdots CHCl^{\beta}]$$
$$\Delta_{rxn}H^{o}_{298.15} \approx -(109 \pm 6)\ \text{kJ}\cdot\text{mol}^{-1} \quad (10)$$

The 1,3-dichloro-1-propen-2-yl radical may isomerize to 1,3-dichloroallyl radical through hydrogen transfer

$$CH_2Cl^{\gamma}-\dot{C}=CHCl^{\beta} \xrightarrow{3,2\text{-H}} \cdot[CHCl^{\gamma}\cdots CH\cdots CHCl^{\beta}]$$
$$\Delta_{rxn}H^{o}_{298.15} = -(116 \pm 6)\ \text{kJ}\cdot\text{mol}^{-1} \quad (11)$$

Gas chromatography has detected chloroallene among the end products of Cl + propargyl chloride. This observation establishes the activity of the Cl atom elimination channel from the 1,3-dichloro-1-propen-2-yl radical

$$CH_2Cl^{\gamma}-\dot{C}=CHCl^{\beta} \rightarrow CH_2=C=CHCl^{\beta} + \cdot Cl^{\gamma}$$
$$\Delta_{rxn}H^{o}_{298.15} = +(73 \pm 6)\ \text{kJ}\cdot\text{mol}^{-1} \quad (12)$$

Although endothermic, reaction **12** may occur because the activated 1,3-dichloro-1-propen-2-yl radical contains energy sufficient to proceed through the net reaction

$$CH_2Cl^{\gamma}-C\equiv CH + \cdot Cl^{\beta} \rightarrow CH_2=C=CHCl^{\beta} + \cdot Cl^{\gamma}$$
$$\Delta_{rxn}H^{o}_{298.15} = -(7 \pm 6)\ \text{kJ}\cdot\text{mol}^{-1} \quad (13)$$

Computational Methods and Terminology. All calculations[13] described herein were carried out with the Gaussian 94 and Gaussian 98 program suites[14,15] on a Cray C90/6256 supercomputer and a 32-processor Silicon Graphics Origin 2000 parallel computer. Fully optimized geometries of reactants, intermediate stationary structures (designated with "IS" prefixes), transition state structures (designated with "TS" prefixes), and products were calculated with the unrestricted second-order Møller−Plesset perturbation theory (UMP2),[16] the hybrid three parameter B3LYP density functional theory,[17] and the quadratic configuration interaction (QCISD) method,[18] including single and double electronic excitations. All calculations were carried out using the 6-31+(d,p) basis set.[19−23] In this work, we follow the standard notation "Theory/basis" to indicate that a full geometry optimization has been carried out at the "Theory" level using the "basis" basis set. In addition, the terms "Theory2/basis2//Theory1/basis1" are used to indicate a single point energy calculation at the "Theory2/basis2" level of theory using the geometry previously optimized at the "Theory1/basis1" level.

We use H^{MP2}, H^{B3LYP}, and H^{QCISD} to denote the electronic energies of the fully optimized structures obtained at the MP2/6-31+G(d,p) and B3LYP/6-31+(d,p), QCISD/6-31+G(d,p) levels, respectively. We use H^{PMP2} to denote the spin-projected electronic energy at the fully optimized MP2/6-31+G(d,p) geometry after the spin-contamination is reduced to a minimum using the method of Schlegel.[24−27] In addition, single point calculations with the 6-311+G(d,p) basis were carried out at the quadratic configuration interaction level including double electron excitations and a perturbative correction for triple excitations, (QCISD(T)/6-311+G(d,p)), using the fully optimized MP2, B3LYP, and QCISD geometries. The electronic energies obtained from these calculations are denoted $H^{Q(T)//MP2}$, $H^{Q(T)//B3LYP}$, and $H^{Q(T)//QCISD}$, respectively. Reaction pathways were computed by the IRC algorithm of Gonzalez and Schlegel,[28−30] as implemented in the G94 and G98 program suites.[14,15] Harmonic vibrational frequencies and zero point energy corrections, $(H_0^{ZPE})^{Level}$, were computed at the MP2/6-31+G(d,p), B3LYP/6-31+(d,p), and QCISD/6-31+(d,p) levels. All computational results, presented herein, contain no empirical scaling of vibrational frequencies and zero point energies.

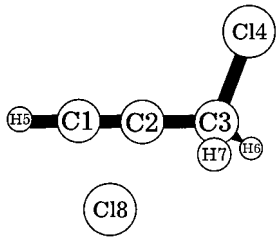

Figure 1. Schematic of the Cl + propargyl system showing the numbering system for the atoms referenced in Supplementary Table 2S and in the *x*-axis of the figures.

In some figures we plot $\Delta_{path}H^{Level}$, the electronic energy of the IRC reaction path relative to the electronic energies of propargyl chloride and the chlorine atom. We note that $\Delta_{path}H^{Level}$ does not include zero point energy contributions. When zero point energy is accounted, we quote $\Delta_{rel}H_0^{Level}$, the energy at 0 K of a stationary point relative to the initial reactants, Cl + propargyl chloride. For example where

$$\Delta_{rel}H_0^{Q(T)//MP2}(TS) = H_0^{Q(T)//MP2}(TS) - H_0^{Q(T)//MP2}(C_3H_3Cl) - H_0^{Q(T)//MP2}(Cl)$$

$$H_0^{Q(T)//MP2} = H^{Q(T)//MP2} + (H_0^{ZPE})^{MP2}$$

Results

Thermochemical Properties and Geometry Parameters. For each stable molecule and persistent radical found in reactions 2 through 13 Table 1 lists the $\Delta_f H^o_T$ used to derive the reaction enthalpies of reactions **2**−**13**. Supplementary Table 1S lists $H^{Q(T)//QCISD}$, the electronic energy, and $(H_0^{ZPE})^{MP2}$, the zero point energy correction computed at the MP2/6-31+G(d,p) level. The energy diagrams presented in this paper are based solely on ab initio results. To save considerable computational resources, we use $(H_0^{ZPE})^{MP2}$ in derivations of $\Delta_{rel}H_0^o$ for the persistent species (Table 1S). Substitution of $(H_0^{ZPE})^{MP2}$ for $(H_0^{ZPE})^{QCISD}$ (or $(H_0^{ZPE})^{B3LYP}$ for $(H_0^{ZPE})^{QCISD}$) is expected to introduce negligible relative error. The NIST Computational Chemistry Comparison and Benchmark DataBase[31] lists QCISD/6-31G(d), MP2/6-31G(d), and B3LYP/6-31G(d) vibrational frequency data sets for nine chlorinated molecules.[32] The zero point energies computed for these data sets differ by ∼1%.

During this study, we found nine transition states and four intermediate structures associated with reactions **2**−**12**. Figure 1 displays the atom numbering system used in this report for geometry descriptions of the transition states and intermediate structures. Supplementary Table 2S lists the fully optimized geometries obtained at the highest level of theory used in this work, the QCISD/6-31+G(d,p) geometry. Fully optimized geometries obtained at other levels differ only slightly from those listed in Supplementary Table 2S and are not reported. Supplementary Table 2S also lists the electronic energy at the highest level of calculation (usually $H^{Q(T)//QCISD}$), H_0^{ZPE}, and the $\nu_i^{\ddagger}$, the imaginary frequency corresponding to the transition state. Table 2 lists $\Delta_{rel}H_0^{Level}$(TS), the energy at 0 K of the transition state relative to the initial reactants, Cl + propargyl chloride.

TABLE 2: Energy of Transition States Relative to the Initial Reactants, Cl + Propargyl Chloride, Determined at Seven Levels of Theory[h]

calculation level	TS3	TS4	TS7c	IS7p	IS7n	TS7e	TS8	TS9	TS10r	TS10a	IS10b	TS10v	TS11
$\Delta_{rel}H_0^{Q(T)//QCISD}$[a] kJ·mol^{-1}	5	124[b]	−6	−11	−10	−6	[c]	95[b]	−93[b]	−7	−10	−14	119[d]
$\Delta_{rel}H_0^{Q(T)//MP2}$ kJ·mol^{-1}	16	132	2	−8	−8	2	[e]	102	−89	8		1	[f]
$\Delta_{rel}H_0^{Q(T)//B3LYP}$ kJ·mol^{-1}	8	113	−9	[f]	[f]	[f]	113	86	−109	−11		[f]	119
$\Delta_{rel}H_0^{QCISD}$[a] kJ·mol^{-1}	24	130[b]	2	−3	−2	1	[c]	115[b]	−91[b]	−3	−9	−7	136[d]
$\Delta_{rel}H_0^{PMP2}$[g] kJ·mol^{-1}	19 $\langle S^2\rangle_p$= 0.76	125 $\langle S^2\rangle_p$= 0.81	5 $\langle S^2\rangle_p$= 0.77	−8 $\langle S^2\rangle_p$= 0.75	−6 $\langle S^2\rangle_p$= 0.75	4 $\langle S^2\rangle_p$= 0.77	[e]	103 $\langle S^2\rangle_p$= 0.77	−88 $\langle S^2\rangle_p$= 0.75	9 $\langle S^2\rangle_p$= 0.77	−4 $\langle S^2\rangle_o$= 0.75	1 $\langle S^2\rangle_p$= 0.79	[e]
$\Delta_{rel}H_0^{MP2}$ kJ·mol^{-1}	45 $\langle S^2\rangle_o$= 0.88	176 $\langle S^2\rangle_o$= 1.0	37 $\langle S^2\rangle_o$= 0.93	−7 $\langle S^2\rangle_o$= 0.76	−6 $\langle S^2\rangle_o$= 0.76	36 $\langle S^2\rangle_o$= 0.93	[e]	138 $\langle S^2\rangle_o$= 0.95	−81 $\langle S^2\rangle_o$= 0.80	40 $\langle S^2\rangle_o$= 0.94	−1 $\langle S^2\rangle_o$= 0.76	39 $\langle S^2\rangle_o$= 0.99	[e]
$\Delta_{rel}H_0^{B3LYP}$ kJ·mol^{-1}	−22	48	−31	[f]	[f]	[f]	84	75	−119	−54	[f]	[f]	94

[a] Except as noted, the relative energy contains $(H_0^{ZPE})^{QCISD}$. See text. [b] Computed using $(H_0^{ZPE})^{MP2}$. [c] QCISD/6-31+G(d,p) structure calculation did not converge to a unique geometry. See text. [d] Computed using $(H_0^{ZPE})^{B3LYP}$. [e] MP2/6-31+G(d,p) structure calculation did not converge to a unique geometry. See text. [f] B3LYP/6-31+G(d,p) calculation found no evidence of a stationary structure. See text. [g] Computed with $H_0^{PMP2} = H^{PMP2} + (H_0^{ZPE})^{MP2}$ evaluated at the fully optimized MP2/6-31+G(d,p) geometry. [h] The total spin expectation value, $\langle S^2\rangle$, is listed for the PMP2 and MP2 relative energies of each stationary structure.

TABLE 3: Arrhenius and Activation Coefficients of the High Pressure Rate Equation, $k_\infty = A\cdot e^{-Ea/RT}$, for Each Elementary Reaction of the Cl + Propargyl Chloride System, Computed with Cannonical Transition State Theory from the ab Initio Results

rxn	$A_{forward}$, cm^3·s^{-1}	$(E_a)_{forward}$, kJ·mol^{-1}	$A_{reverse}$, cm^3·s^{-1}	$(E_a)_{reverse}$, kJ·mol^{-1}
3	$(1.2 \times 10^{-11})^a$	7	$(3.8 \times 10^{-13})^a$	86
4	$(3.0 \times 10^{-11})^a$	127	$(9.9 \times 10^{-14})^a$	90
5	$(1.7 \times 10^{-10})^a$	0	3.4×10^{15}	75
6	$(1.8 \times 10^{-10})^a$	0	1.5×10^{15}	77
7	4.6×10^{13}	71	1.9×10^{13}	73
8	1.1×10^{13}	194	1.1×10^{13}	303
9	1.5×10^{12}	171	1.5×10^{12}	280
10	5.1×10^{12}	62	1.2×10^{13}	169
11	3.3×10^{13}	196	3.3×10^{13}	314
12	1.7×10^{15}	75	$(5.1 \times 10^{-10})^a$	0

[a] Bimolecular coefficient in units of cm^6·s^{-1}.

Table 2 lists these predicted relative energies at the seven computational levels used in this study.

Using cannonical transition state theory[33−35] as implimented in the CHEMRATE program,[9] the ab initio results were used to derive high-pressure rate expressions at 298 K. Table 3 lists the Arrhenius and activation coefficients for the high-pressure rate equation of the form, $k_\infty = A\cdot e^{-Ea/RT}$. To derive coefficients, we adopted the approximation, $E_a \approx \Delta_{rel}H_0^{Q(T)//QCISD}$ at 0 K. Arrhenius coefficients are estimated using the geometries and vibrational frequencies of persistent species and transition states, computed at the MP2/6-31+G(d,p) level and reduced by a scaling factor of 0.937 (Table 3S). Hindered internal rotors and tunneling are not considered. For reactions **5**, **6**, and **−12**, the present ab initio calculations found no transition structures. To estimate the high-pressure rate equations for these barrierless reactions, we obtained program input by devising an approximate transition state structure and spectrum, and by defining the corresponding enthalpy of formation to obtain the zero activation energy. This procedure appears to give reasonable high-pressure rate constants at 298 K because the Arrhenius coefficient of metathesis reaction **3** is similar to the corresponding coefficient reported for Cl + propyne metathesis,[36] k_5 and k_6 are within an order of magnitude of k(Cl + C_3H_3Cl) at 625 Pa,[8] which is in the pressure falloff region, and k_{12} is the same as observed for k(Cl + allene) near the high-pressure limit.[37] The k_∞'s provide a map of the intrinic barriers and give a sense of the relative tightness of the transition states. However, because the Cl + propargyl chloride addition reaction is governed by chemically activated $C_3H_3Cl_2$ ensembles that manifest nonthermal energy distributions, elementary k_∞ do not predict the overall reaction in the pressure falloff region. The predicted product distributions from chemically activated $C_3H_3Cl_2$ complexes are presented in the Discussion.

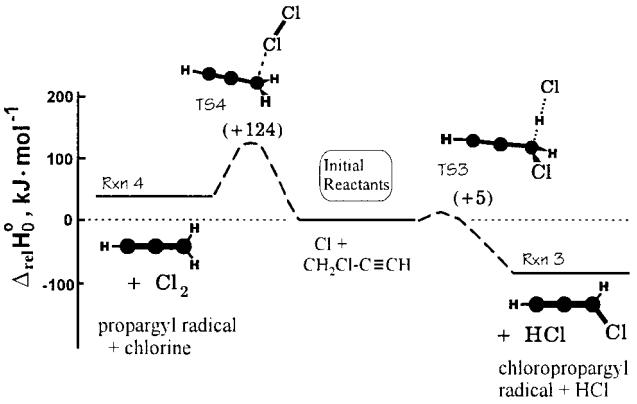

Figure 2. Reaction energy diagram at 0 K of metathesis reaction channels accessible as a chlorine atom approaches propargyl chloride. Reaction enthalpies are referenced to the reactants (Cl + $CH_2ClC{\equiv}CH$) at 0 K. The values listed in parentheses are the ab initio $\Delta_{rel}H_0^{Q(T)//QCISD}$ (in kJ·mol^{-1}) of the transition state structures, which include unscaled zero point energy contributions.

Metathesis and Addition Channels. Metathesis reactions **3** and **4** involve direct attack by a chlorine atom followed by an abstraction of a hydrogen atom (going through TS3) or a chlorine atom (going through TS4) from the chloromethyl group in propargyl chloride. Figure 2 diagrams the potential energy profiles for these reactions. The results in Figure 2 show that the barrier to hydrogen abstraction, $\Delta_{rel}H_0^{Q(T)//QCISD}$(TS3), lies 5 kJ·mol^{-1} above reactants. Similar QCISD(T)/6-311+G(d,p)//QCISD/6-31+G(d,p) calculations predict a relatively large barrier for the chlorine abstraction channel ($\Delta_{rel}H_0^{Q(T)//QCISD}$(TS4) = 124 kJ·mol^{-1}). This study does not consider reaction **2** because its reaction is $\Delta_{rxn}H_0^o \approx 100$ kJ·mol^{-1} endothermic,

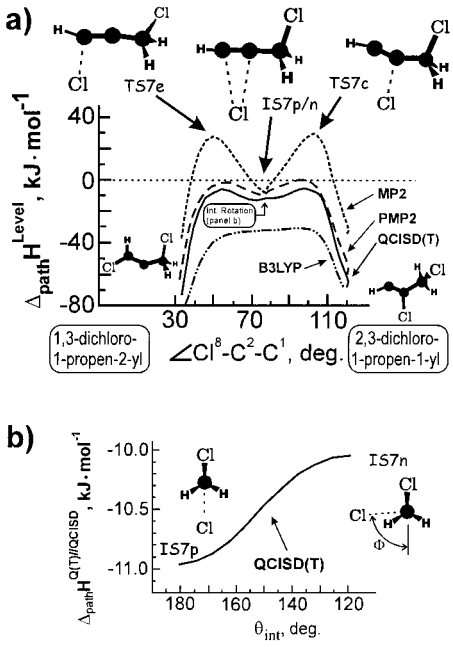

Figure 3. Energy profile governing chlorine atom transfer between 1,3-dichloro-1-propen-2-yl radical and 2,3-dichloro-1-propen-1-yl radical (reaction **7**) predicted by ab initio calculations. Energies are referenced to the separated Cl atom and propargyl chloride energies at the corresponding computational theory level and do not include zero point energy contributions. a) $\Delta_{path}H^{Level}$ as a function of $\angle(Cl^8-C^2-C^1)$. The trace labeled QCISD(T) is an estimate derived by interpolating the MP2 trace so that it intersects the $\Delta_{path}H^{Q(T)/QCISD}$ computed for each diagrammed (stationary) structure. b) Energy profile of $\Delta_{path}H^{Q(T)/QCISD}$ as a function of the internal rotation coordinate, θ_{int}, where $\theta_{int} \equiv \angle(Cl^8-C^2-C^3-Cl^4)$. This internal rotation, involving the Cl atom, links IS7p and IS7n near $\angle(Cl^8-C^2-C^1) = 79°$, as indicated in panel a).

making it unimportant to the reaction mechanism at 298 K. To examine chlorine addition reactions **5** and **6**, we conducted a series of relaxed potential energy scans at the B3LYP and MP2 levels of theory as a function of carbon−chlorine distance. These scans demonstrated that the relative energy diminishes continuously as the chlorine−carbon internuclear distance decreases from 4 Å to the equilibrium distance (∼1.8 Å). The lack of a transition state indicates that the chlorine addition reactions **5** and **6** are barrierless processes. Given that both addition reactions have negligible energy barriers and that the metathesis reactions have energy barriers, we expect chlorine addition to dominate the reactivity at low temperatures. The incipient products of Cl + propargyl are ensembles of 2,3-dichloro-1-propen-1-yl and 1,3-dichloro-1-propen-2-yl radicals.

Following the formation of the chemically activated $C_3H_3Cl_2$ ensemble through chlorine addition, exothermic HCl elimination could conceivably proceed through 3-, 4-, and 5-center transition state structures. However, preliminary explorations for these transition structures from the 2,3-dichloro-1-propen-1-yl, 1,3-dichloro-1-propen-2-yl, 1,2-dichloroallyl, and 1,3-dichloroallyl radicals were unsuccessful. Exhaustive ab initio searches for these metathesis channels were not pursued.

Isomerization Reaction of the 2,3-Dichloro-1-propen-1-yl Radical. At 0 K, each incipient 2,3-dichloro-1-propen-1-yl radical forms with $E_v \approx 78$ kJ·mol^{-1} of internal vibrational energy. Calculations indicate that this internal energy is sufficient to promote isomerization reaction **7**, which converts 2,3-dichloro-1-propen-1-yl radicals into the 1,3-dichloro-1-propen-2-yl radicals. Figure 3a diagrams the energy profile of the 2,3-Cl atom transfer (reaction **7**) by plotting $\Delta_{path}H^{Level}$, the electronic energy (containing no ZPE contributions) relative to Cl + propargyl chloride, as a function of $\angle Cl^8-C^2-C^1$ angle. In Figure 3a, we constructed the profile labeled MP2 using internal reaction coordinate (IRC) calculation data[28−30] at the MP2/6-31+G(d,p) level. The trace labeled PMP2 shows the electronic energy of each MP2/6-31+G(d,p) structure after full annihilation of spin-contaminants. The isomerization path passes through two distinct transition state structures, labeled TS7c and TS7e (Table 2S). TS7c ($\angle Cl^8-C^2-C^1 = 100.9°$) resembles the 2,3-dichloro-1-propen-1-yl radical ($\angle Cl^8-C^2-C^1 \approx 120°$) except that all non-hydrogen atoms lie in the same plane and the C−Cl bond is lengthened to $r(C^2-Cl^8) = 2.354$ Å. TS7e ($\angle Cl^8-C^2-C^1 = 52.9°$) is similar to the 1,3-dichloro-1-propen-2-yl radical ($\angle Cl^8-C^2-C^1 \approx 33°$) except that the C−Cl bond is lengthened to $r(C^3-Cl^8) = 2.385$ Å.

Midway between TS7c and TS7e ($\angle Cl^8-C^2-C^1 \approx 79°$), $\Delta_{path}H^{Level}$ decreases as the reaction path passes through minimum energy structures, IS7p and IS7n (Table 2S). IS7p and IS7n are stationary intermediate structures exhibiting only real vibrational frequencies. Both IS7p and IS7n have a chlorine atom bridging between C^3 and C^2 with nearly equal bond lengths, $r(C^1-Cl^8) \approx 3$ Å (Figure 2a). However, IS7p and IS7n differ with respect to the placement of the chlorine atom relative to the plane containing the other non-hydrogen atoms. In IS7p all heavy atoms lie in the same plane ($\theta_{int} = 180°$, where $\theta_{int} \equiv \angle Cl^8-C^2-C^3-Cl^4$). In IS7n the bridging chlorine is rotated above the heavy-atom plane to $\theta_{int} = 94.3°$. Figure 3b plots $\Delta_{path}H^{Q(T)//QCISD}$ as a function of θ_{int}, (where $\theta_{int} \equiv \angle Cl^8-C^2-C^3-Cl^4$)), showing that the path between IS7p and IS7n contains no energy barrier. The QCISD(T)/6-311+(d,p)//QCISD/6-31+(d,p) calculations find that IS7n is about 1 kJ·mol^{-1} less stable than IS7p. IRC calculations confirmed that the 2,3-dichloro-1-propen-1-yl and 1,3-dichloro-1-propen-2-yl radicals also lie on the same reaction path as TS7c, IS7p, IS7n, and TS7e.

The energy barriers predicted for reaction **7** vary as a function of the level of theory. The MP2/6-31+G(d,p) calculations predict that TS7c and TS7e lie about $\Delta_{rel}H_0^{MP2} \approx +36$ kJ·mol^{-1} above reactants (Table 2); however, the MP2 wave functions contain large amounts of spin contamination ($\langle S^2\rangle_o = 0.93$), suggesting that these MP2 barriers might be unreliable. Full annihilation of spin contaminants at the MP2/6-31+G(d,p) geometries ($\langle S^2\rangle_p = 0.77$) predict much lower barriers, $\Delta_{rel}H_0^{PMP2} \approx +4$ kJ·mol^{-1} (We note that the PMP2 reaction path also exhibits minima at IS7p and TS7n.) The QCISD/6-31+G(d,p) calculations also find TS7c, IS7p, IS7n, and TS7e but predict that these structures are nearly thermoneutral relative to Cl + propargyl chloride. In contrast, the B3LYP/6-31+G(d,p) calculations found only TS7c, rather than four stationary points along the reaction path. At this level TS7c is a low energy barrier, $\Delta_{rel}H_0^{B3LYP} \approx -31$ kJ·mol^{-1}, which we judge as unreliable due to the known propensity of density functional methods for underestimating energy barriers.

To estimate more reliable energy barriers, we reoptimized the stationary structures, TS7c, IS7p, IS7n, TS7e, and both stable radicals, at the QCISD/6-31+G(d,p) level and computed the energy of each structure at the QCISD(T)/6-311+G(d,p) level (Table 2S). To plot estimated energy profiles at this higher level, we computed $\Delta_{path}H^{Q(T)//QCISD}$ at each stationary point and then scaled and interpolated the MP2 IRC path so that it intersects these $\Delta_{path}H^{Q(T)//QCISD}$. The energy profiles of Figure 3 labeled QCISD(T) show that the complete reaction path lies at lower energy than Cl + propargyl chloride. When zero point energy corrections are included in the calculation of TS7c and TS7e, the calculations give $\Delta_{rel}H_0^{Q(T)//QCISD} = -6$ kJ·mol^{-1} (Table 2).

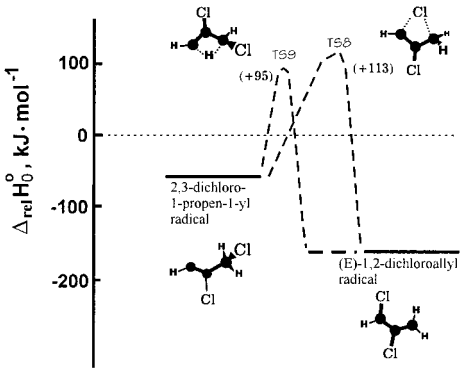

Figure 4. Reaction energy diagram at 0 K of the chlorine atom transfer (reaction **8**) and hydrogen atom transfer (reaction **9**) channels that isomerize 2,3-dichloro-1-propen-1-yl radical into 1,2-dichloroallyl radical. Reaction enthalpies are referenced to the separated Cl atom and propargyl chloride at 0 K. The values listed in parentheses are the ab initio $\Delta_{rel}H_0^{Q(T)//QCISD}$ (in kJ·mol^{-1}) of the transition state structures, which include unscaled zero point energy contributions.

Thus, we predict that isomerization reactions **7** and −**7** proceed are active the chemically activated C_3H_3Cl complex.

Reactions **8** and **9** isomerize 2,3-dichloro-1-propen-1-yl radical into 1,2-dichloroallyl radical through 1,3-transfers of a chlorine or hydrogen atom, respectively. Figure 4 diagrams the predicted transition state structures and reaction enthalpies. A B3LYP/6-31+G(d,p) calculation found TS8, the transition state structure for chlorine transfer. To estimate the reaction energy, we computed the necessary electronic energies at the QCISD-(T)/6-311+G(d,p)//B3LYP/6-31+G(d,p) level and zero point energies at the B3LYP/6-31+G(d,p) level. The results indicate that $\Delta_{rel}H_0^{Q(T)//B3LYP}(TS8) = 113$ kJ·mol^{-1}, indicating that the intrinsic barrier for this process lies above the initial reactants. We note that the geometry optimizations of TS8 at the MP2 and QCISD levels did not converge. Because these MP2 and QCISD structure calculations attempted to converge to a geometry similar to the B3LYP structure and since additional calculations seemed unlikely to make the relative energy of TS8 exothermic relative to Cl + propargyl chloride, we did not pursue the MP2 and QCISD geometry optimizations further. Although the reasons for the odd behavior of MP2 and QCISD in the optimization of TS8 are not well understood, it is possible that spurious couplings in the updated Hessian during the optimizations at these two levels may have led the optimizer to move around the basin of attraction located at TS8 without converging. This problem could arise if the region of the potential energy surface surrounding TS8 is significantly flat. One way of confirming this proposal is to carry full geometry optimizations of TS8 with smaller step sizes, tighter convergence criteria, and using Hessian matrixes computed analytically at every point on the optimization. However, this process could become prohibitively expensive (especially at the QCISD level).

The geometry of TS9 was obtained with a QCISD/6-31+G-(d,p) calculation (Table 2S). Formation of TS9 is also very endothermic, $\Delta_{rel}H_0^{Q(T)//QCISD}(TS9) = 95$ kJ·mol^{-1}, relative to Cl + propargyl chloride. Because TS8 and TS9 reside at high energy relative to the reactants, we do not expect reactions **8** and **9** to contribute to the overall reaction mechanism at 298 K.

Isomerization and Dissociation Reactions of the 1,3-Dichloro-1-propen-2-yl Radical. *Ab initio* calculations predict that chemically activated 1,3-dichloro-1-propen-2-yl radicals contain sufficient energy to isomerize into 1,2-dichloroallyl radicals by transferring a chlorine atom between the end and

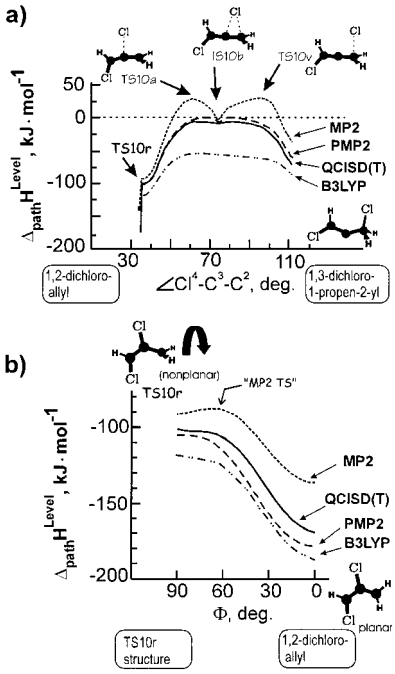

Figure 5. Energy profile governing chlorine atom transfer between 1,3-dichloro-1-propen-2-yl radical and 1,3-dichloroallyl radical (reaction **10**) predicted by ab initio calculations. Energies are referenced to the separated Cl atom and propargyl chloride energies at the corresponding computational theory level and do not include zero point energy contributions. (a) $\Delta_{path}H^{Level}$ as a function of ∠(Cl^4−C^3−C^2). The trace labeled QCISD(T) is an estimate derived by interpolating the MP2 trace so that it intersects the $\Delta_{path}H^{Q(T)//QCISD}$ computed for each diagrammed structure. b) Energy profile of $\Delta_{path}H^{Level}$ as a function of the internal rotation of the CH_2 group plane relative to the plane of the heavy atoms of the $C_3H_3Cl_2$ radical. This links TS10r with the 1,2-dichloroallyl radical.

center carbon atoms (reaction **10**). Figure 5a diagrams the energy profile of the 3,2-Cl atom transfer by plotting $\Delta_{path}H^{Level}$, the electronic energy relative to Cl + propargyl chloride, as a function of ∠Cl^4−C^3−C^2 angle. Figure 5b plots $\Delta_{path}H^{Level}$ as a function of about Φ, which is defined as the angle of the C^3H_2 plane relative to the heavy atom plane (i.e., $\Phi \equiv 90° + (\angle C^1{-}C^2{-}C^3{-}H^7 + \angle C^1{-}C^2{-}C^3{-}H^8)/2$). The profile labeled MP2 was constructed using internal reaction coordinate (IRC) calculation data[28−30] at the MP2/6-31+G(d,p) level that traced the reaction paths from the transition states, TS10v and TS10a. The PMP2 trace plots the energies of the MP2/6-31+G(d,p) structures along the IRC path after annihilation of spin-contamination. The trace labeled B3LYP is the reaction path extending from TS10a obtained from an IRC calculation at the B3LYP/6-31+G(d,p) level. To construct the path labeled QCISD(T), we re-optimized the stationary structure geometries of TS10r, TS10a, IS10b, TS10v, and both stable radicals at the QCISD/6-31+G(d,p) level and computed single point QCISD-(T)/6-311+G(d,p) energies for these geometries. We then scaled and interpolated the B3LYP profile so that it intersects the $\Delta_{path}H^{Q(T)//QCISD}$ computed for each stationary structure. We note that $\Delta_{path}H^{Level}$ does not contain zero point energy contributions.

From the 1,3-dichloro-1-propen-2-yl radical the reaction path follows coordinate ∠(Cl^4−C^3−C^2), passing through transition states TS10v and TS10a (Figure 5a), and intersects a third transition state, labeled TS10r, where the reaction path changes over to follow coordinate Φ (Figure 5b). TS10v (∠Cl^4−C^3−C^2 = 95.9°) resembles the 1,3-dichloro-1-propen-2-yl radical (∠Cl^4−C^3−C^2 = 64.7°) except that the C−Cl bond is length-ened to r(C^3−Cl^4) = 2.432 Å. The reaction path extending from

TS10v terminates at the 1,3-dichloro-1-propen-2-yl radical and at IS10b. TS10a ($\angle Cl^4-C^3-C^2 = 35.9°$) resembles the 1,2-dichloroallyl radical ($\angle Cl^4-C^3-C^2 = 34.9°$) but features a lengthened C−Cl bond ($r(C^3-Cl^4) = 2.855$ Å) and the CH_2 group plane is rotated 90° relative to the heavy atom plane. The reaction path from TS10a terminates at TS10r and IS10b. IS10b ($\angle Cl^4-C^3-C^2 = 74.5°$) contains a chlorine atom bridging across carbons C^2 and C^3 with nearly equal bonds of $r(C^i-Cl^4) \approx 2.9$ Å. TS10r closely resembles the 1,2-dichloroallyl radical except that the CH_2 group plane is rotated 90° relative to the heavy-atom plane. From TS10r, rotation of the C^3H_2 group from $\Phi = 90°$ to $\Phi = 0°$ provides −62 kJ mol^{-1} of stabilization energy and transforms the $C_3H_3Cl_2$ complex into the planar 1,2-dichloroallyl radical (Figure 5b). In summary, the IRC calculations at the MP2 and B3LYP levels show that a continuous path links the 1,3-dichloro-1-propen-2-yl and 1,2-dichloroallyl radicals through reaction **10**. The lengthened C−Cl bond length and absence of resonance stabilization accounts for the relatively high energies of the TS10v, IS10b, and TS10a stationary structures (Table 2S).

IS10b and TS10v probably do not exist in the true path of reaction **10**, leaving TS10a as the governing barrier. This conclusion is supported by the difficulties encountered while characterizing IS10b and TS10v at the MP2/6-31+G(d,p) and QCISD/6-31+(d,p) levels. Although the IRC calculations at the MP2/6-31+G(d,p) level initiated at the TS10a and TS10v geometries terminated at similar IS10b geometries, these structures were not identical. Attempts to reoptimize these IS10b structures failed to converge. However, we note that at the QCISD(T)/6-311+G(d,p) level the relative energy near IS10b becomes greater than at TS10v, i.e., $\Delta_{path}H^{Q(T)//QCISD}$ (IS10b) = −13 kJ·mol^{-1}, $\Delta_{path}H^{Q(T)//QCISD}$ (TS10v) = −14 kJ·mol^{-1}, and $\Delta_{path}H^{Q(T)//QCISD}$ (TS10a) = −9 kJ·mol^{-1}). This suggests that calculations that capture all correlation energy will not find a first-order saddle point at TS10v. We conclude that reaction **10** is governed only by TS10a. When zero point energies are included, the highest level calculations predict $\Delta_{rel}H_0^{Q(T)//QCISD}$ (TS10a) = −7 kJ·mol^{-1}. Thus, we predict that isomerization reaction **10** is active in the chemically activated C_3H_3Cl complex.

Figure 5b plots $\Delta_{path}H^{Level}$ as a function of Φ, where Φ is the angle of the CH_2 plane relative to the plane containing the carbon atoms ($\Phi \equiv 90° - (\angle(H^6-C^3-C^2-C^1) + \angle(H^7-C^3-C^2-C^1))/2$). The plot shows that ∼62 kJ·mol^{-1} resonance stabilization realized as TS10r ($\Phi = 90°$) becomes 1,2-dichloroallyl radical ($\Phi = 0°$). At the QCISD/6-31+G(d,p) level and B3LYP/6-31+G(d,p) levels rotation of the CH_2 group into the heavy atom plane (i.e., $\Phi \rightarrow 0°$) is a barrierless process. In contrast, the MP2/6-31+G(d,p) calculations predict a 3 kJ·mole^{-1} C^3H_2 rotational barrier at $\Phi \approx 66°$ (labeled "MP2 TS" in Figure 5b). Spin contamination appears to account for this transition state in the MP2/6-31+G(d,p) energy profile. The fully optimized structures used to construct the $\Delta_{path}H^{MP2}$ profile in Figure 5b manifest unprojected spin eigenvalues of $\langle S^2\rangle_o \approx 0.86$. When spin contaminants are eliminated from the wave function using the PMP2 spin projection method of the GAUSSIAN program, the corresponding $\Delta_{path}H^{PMP2}$ profile steadily decreases with decreasing Φ and exhibits no energy maximum.

Figure 6 diagrams the energy relationships of structures involved with the remaining reaction channels available to 1,3-dichoro-1-propen-2-yl radical. The 1,3-dichloro-1-propen-2-yl radical may isomerize through TS11 forming 1,3-dichloroallyl radical by transferring a hydrogen atom from the chloromethyl group to the center carbon. The ab initio results find

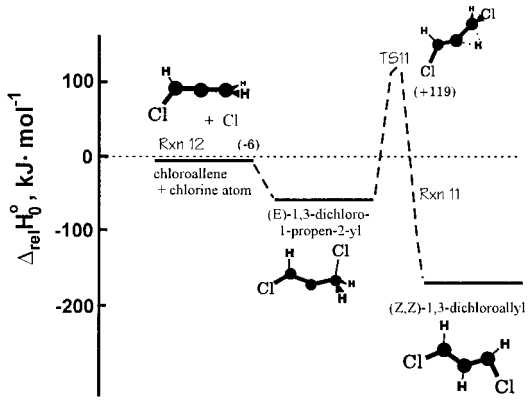

Figure 6. Reaction energy diagram at 0 K showing channels that may deplete 1,3-dichloro-1-propen-2-yl radical through hydrogen transfer (reaction **11**) or dissociation (reaction **12**). Reaction enthalpies are referenced to the separated Cl atom and propargyl chloride at 0 K. The values listed in parentheses are the ab initio $\Delta_{rel}H_0^{Q(T)//QCISD}$ (in kJ·mol^{-1}) of the transition state structures, including unscaled zero point energy contributions.

$\Delta_{rel}H_0^{Q(T)//QCISD}$ (TS11) = 119 kJ·mol^{-1}, indicating that the formation of TS11 from Cl + propargyl chloride is an endothermic process. Therefore, reaction **11** does not contribute to the overall reaction mechanism at ambient temperature.

To investigate chlorine−carbon bond scission in the chloromethyl group of 1,3-dichloro-1-propen-2-yl radical (reaction **12**), a series of fully optimized structures were computed at the MP2 and B3LYP levels as the $r(C^3-Cl^4)$ distance increased from the equilibrium distance ($r(C^3-Cl^4) \approx 1.8$ C). Because the total energy increased continuously as the chlorine−carbon internuclear distance was increased, we conclude that reaction **12** has no transition structure and the chlorine atom elimination is a barrierless process. Since reaction **12** is slightly exothermic, chloroallene is expected to appear among the stable end-products of Cl + propargyl chloride.

Discussion

By using high level ab initio calculations, this study has computed nine transition state structures and four intermediate structures involving eleven elementary reactions of the Cl + propargyl chloride reaction. Despite the differences in the energetics obtained by the different methods used in this study (MP2, PMP2, B3LYP, QCISD, and QCISD(T)), each level predicts essentially the same reaction mechanism for chlorine atom with propargyl chloride. These results provide significant confidence in the proposed mechanisms.

Ab Initio Results. The collective results highlight the important influences of spin contamination and correlation upon predicted energy barriers. For most barriers (e.g., TS3, TS4, TS7c, TS7e, TS9, TS10a, TS10v) spin annihilations in the MP2 wave functions reduce the barrier energies by ∼30 kJ·mol^{-1} (Table 2). Because the MP2 method implemented in most of the available ab initio programs finds optimized molecular structures by using energy gradients based on spin-unprojected wave functions, such calculations are susceptible to spin contamination, inducing artifacts like the "MP2 barrier" found in the isomerization path of reaction **10** (Figure 5b). The importance of correlation is seen by noting that the discord of ∼30 kJ·mol^{-1} among the QCISD, MP2, and B3LYP energy barriers is eliminated by evaluating each structure with a single point QCISD(T)/6−311(d,p) calculation. This observation supports the concept that reliable reaction barriers are estimated efficiently by using a lower level calculation to obtain the

geometry and a high-level QCISD(T)/6−311(d,p) calculation to capture most correlation energy. In summary, the QCISD-(T)/6-311+G(d,p)//QCISD/6-31+G(d,p) method appears to minimize the errors contributing to transition state energy barriers, lending confidence in the verity of the predicted mechanism for the Cl + propargyl chloride reaction.

The issue regarding spin contamination in the QCISD(T) wave function warrants comment. In general, QCISD(T) wave functions based on unrestricted Hartree−Fock wave functions, UHF, are not eigenfunctions of the $\langle \hat{S}^2 \rangle$ spin operator and consequently do not preserve spin symmetry. This immediately leads to the conclusion that QCISD(T) is not exempt of contamination from other spin states. However, for doublets, such as the ones treated in this work, this situation is not critical, given that QCISD(T) should in principle annihilate the principal spin contaminant in the same fashion that Coupled-Cluster in the space of single, double and triple (treated perturbatively) electronic excitations, CCSD(T).[38]

Metathesis Reactions of Cl + Propargyl Chloride. The energy barriers derived from the ab initio results suggest that at 298 K the initial elementary channels of Cl + propargyl chloride have importance in the order of (reaction **5** ≈ reaction **6**) > reaction **3** ≫ reaction **4** ≈ reaction **2**. The high-pressure rate coefficients, computed with transition state theory from the present ab initio results (Table 3), predict the ratio, $k_3/k_{total} \approx 0.002$, for the HCl metathesis vs total bimolecular reactivity at 298 K, where $k_{total} = k_3 + k_4 + k_5 + k_6$. Although the ratio of HCl metathesis and addition reactivity remains unmeasured for Cl + propargyl chloride, we may estimate a ratio at 298 K by examining the available kinetic data for Cl + propyne and then adjusting for the effects of chlorine substitution. By reacting thermal ^{38}Cl atoms with propyne and performing GC analyses of the radioactive products, Lee and Rowland found that chlorine atom addition accounted for >95% of total reactivity between (47 900 to 53 2000) Pa ((360 to 4000) Torr).[39] Prior measurements of chlorine atom reactions with substituted ethanes[40] and propenes[41] have found that the substitution of one chlorine in the methyl group diminishes the metathesis reactivity of *each* chloromethyl hydrogen by a factor of 6 and 10, respectively. Assuming similar scaling for propynes, the fractional reactivity available to HCl metathesis (reaction **2**) for Cl + propargyl chloride is $k_3/k_{total} < 0.01$ at 298 K in the high-pressure limit. Thus, estimates based on ab initio and experimental data indicate that chlorine atom addition (reactions 5 and 6) dominates the reactivity of Cl + propargyl chloride at 298 K.

The present ab initio results give high-pressure rate coefficients predicting the ratio, $k_4/k_{total} \approx 10^{-24}$, for Cl_2 metathesis vs total reactivity at 298 K, i.e., the Cl_2 metathesis channel is inactive. This prediction conflicts with previous interpretations of experiments by Fahr, et al.[42] who proposed a dominant role for reaction **4**. Their experiments photolyzed propargyl chloride with 193 nm light and recorded the transient absorption between 230 and 270 nm. Following the photolysis event, the transient absorption profile exhibited a "prompt" absorption at 242 nm, attributed to the photolytic propargyl radical (C_3H_3) product from reaction **1**, and a more slowly increasing transient absorption, attributed to bimolecular C_3H_3 product from reaction **4**. Because the total absorbance grew to nearly twice the magnitude of the "prompt" absorption, assignment of the 242 nm absorption band to the C_3H_3 radical would imply that the endothermic reaction **4** accounts for ≈ 100% of the Cl + propargyl chloride reactivity. The discord between the interpretions of the ab initio results and of the photolysis experiments suggests that the assignment of the 242 nm absorption band is in error. Evidence that the 242 nm absorption is not carried by the C_3H_3 radical was found by experiments that photolyzed unhalogenated precursors of C_3H_3 radicals (allene and propyne) with 193 nm light and detected no absorption between 230 and 270 nm.[8] In separate experiments, we photolyzed Cl_2 with 355 nm light (to which propargyl chloride is photolytically inert) and demonstrated that the 242 nm absorption arises from a chlorinated product of Cl + propargyl chloride.[8] Thus, the weight of the spectral and kinetic data, the ab initio transition state relative energies, and the computed thermodynamic data (Table 1 and ref 8) establish that reaction **4** is inactive at 298 K. By assigning the spectral carrier as the 1,2-dichloroallyl radical, we can remove the conflict between the present calculations and the prior interpretations of Fahr, et al. The 1,2-dichloroallyl radical is predicted to exhibit a strong transient absorption spectrum between 230 and 270 nm originating from $\tilde{C}(3p) \leftarrow \tilde{X}^2A_2$ transitions.[8] It should be noted that our present assignment does not preclude the existence of weak ($\sigma_{242} < 10^{-20}$ cm^2·molecule^{-1}) underlying absorption from the C_3H_3 radical; however, in the presence of small amounts of 1,2-dichloroallyl radical ($\sigma_{242} = (4.20 \pm 1.05) \times 10^{-17}$ cm^2 molecule^{-1}),[8] such optical absorption will be obscured unless the absorption by the C_3H_3 radical produces a unique signal accessible to an alternate detection method, e.g., photoionization, photelectron, or photofragment spectroscopies.

Reaction Mechanism of Cl + Propargyl Chloride. The absence of significant metathesis contributions at 298 K enables reactions **5** and **6** to dominate the initial Cl + propargyl chloride reaction. Because chlorine atom addition produces chemically activated $C_3H_3Cl_2$ ensembles with energy distributions that are not described by temperatures, thermal rate equations are inappropriate for predicting the product distributions. We have used the master equation solver in the CHEMRATE program[9] to estimate time-dependent product distributions among the $C_3H_3Cl_2$ isomers in the energy transfer region on the basis of RRKM theory for unimolecular reactions. Supplementary Table 3S lists the program input comprising standard enthalpies (Table 1), intrinsic barriers obtained by assuming $E_a \approx \Delta_{rel}H_0^{Q(T)//QCISD}$ at 0 K (Table 2), rotational moments of inertia that are estimated from the optimized QCISD/6-31+G(d,p) geometries (Table 2S), and vibrational frequencies that are estimated with MP2/6-31+G(d,p) calculations and reduced with a 0.937 scaling factor. The present calculations presume that energy transfer collisions between argon and $C_3H_3Cl_2$ radicals conform to the exponential-down model with $\alpha = 500$ cm^{-1}.[43] This value of α is commonly adopted to model shock tube experiments.[44] The time dependent solutions of the relaxation matrix were computed using the Householder algorithm option.

Initial calculations incorporating all elementary reactions of chemically activated $C_3H_3Cl_2$ isomers confirmed emphatically that reactions **8**, **9**, and **11** are effectively inactive for all conditions between 298 and 1000 K and 625−10 000 Pa. Because inclusion of these inactive channels greatly slowed the calculations, the results reported herein incorporate only reactions **5**, **6**, **7**, **10**, and **12**, which are exothermic and have transition state structures at lower energy than the initial reactants (Table 2). This reduced reaction set is depicted in Figure 7.

Table 4 lists the fractional product yields, f_i^m, from $C_3H_3Cl_2$ ensembles prepared by reaction 5, f_i^5, and reaction 6, f_i^6, at 298 and 1000 K for selected pressures of argon, chosen on the basis of available experimental data[8] and representative conditions. Each f_i^m is the temporally integrated fractional yield of collisionally stabilized product "*i*" produced by a chemically

TABLE 4: Master Equation Predictions of f_i^m, the Fractional Product Yields for the $C_3H_3Cl_2$ Ensembles Prepared by Reaction 5 and 6, $\langle p_i \rangle$, Integrated Fractional Yields, and $\langle C_i \rangle$, the Conversion Yield Per Initial Free Chlorine Atom

conditions and initial reactions	fractional yield: Chloroallene	1,2-dichloroallyl radical	1,3-dichloro-1-propen-2-yl radical	2,3-dichloro-1-propen-1-yl radical	Cl + propargyl chloride	HCl + C_3H_2Cl radical
			298 K, 625 Pa			
f_i^5:	0.057	0.015	0.000	0.002	0.926	
f_i^6:	0.678	0.101	0.000	0.000	0.221	
$\langle p_i \rangle$:	0.858	0.135	0.000	0.002		0.005
$\langle C_i \rangle$, molecule·(initial Cl)$^{-1}$	6.05	0.95	0.00	0.02		0.03
			298 K, 1010 Pa			
f_i^5:	0.045	0.020	0.000	0.002	0.932	
f_i^6:	0.600	0.218	0.001	0.000	0.180	
$\langle p_i \rangle$:	0.725 (0.75)[a]	0.267 (0.24)[a,b]	0.002 (<0.01)[a,c]	0.002		0.004
$\langle C_i \rangle$, molecule·(initial Cl)$^{-1}$	2.63	0.97	0.01	0.01		0.02
			298 K, 10000 Pa			
f_i^5:	0.043	0.018	0.000	0.002	0.937	
f_i^6:	0.585	0.245	0.002	0.000	0.168	
$\langle p_i \rangle$:	0.70	0.29	0.00	0.00		0.00
$\langle C_i \rangle$, molecule·(initial Cl)$^{-1}$	2.32	0.97	0.01	0.01		0.01
			1000 K, 1010 Pa			
f_i^5:	0.059	0.000	0.000	0.000	0.941	
f_i^6:	0.877	0.000	0.000	0.000	0.123	
$\langle p_i \rangle$:	0.97	0.00	0.00	0.00		0.03
$\langle C_i \rangle$, molecule·(initial Cl)$^{-1}$	30.89	0.00	0.00	0.00		1.00

[a] Product distribution measured by static bulb experiments reported in ref 8. See text. [b] 1,2-Dichloro-1-propene obtained from hydrogenation of 1,2-dichloroallyl radical. See text and Figure 7. [c] 1,3-Dichloro-1-propene obtained from hydrogenation of 1,3-dichloro-1-propen-2-yl radical. See text and Figure 7.

activated $C_3H_3Cl_2$ ensemble prepared with reaction m at a specified temperature and pressure. The fractional product yields of reaction m are normalized by $\sum_i f_i^m + f_{rev}^m = 1$, where f_{rev}^m is the fraction returned to the initial reactants, Cl + propargyl chloride. Table 4 also lists the integrated fractional yield, corresponding to the distribution of chlorinated products present in a bulb photolysis experiment after the initial concentration of chlorine atoms is depleted. In the absence of recombination and secondary reactions, the integrated fractional yield, $\langle p_i \rangle$, for each product is

$$\langle p_i \rangle = \frac{\sum_m P_m \cdot f_i^m}{1 - \sum_m P_m \cdot f_{rev}^m} \qquad (14)$$

where $P_m = k_m/k_{total}$ (m = 3, 5, 6). For the HCl metathesis reaction **3** we set $f_{HCl}^3 = 1$ and $f_{rev}^3 = 0$ and reaction **4** is not considered. The conversion yield per initial free chlorine atom, $\langle C_i \rangle$, is computed for each set of conditions by dividing each $\langle p_i \rangle$ by the sum of $\langle p_i \rangle$ over the chlorine sequestering products, i.e., the sum of all $\langle p_i \rangle$ except for chloroallene.

The chemically activated $C_3H_3Cl_2$ ensembles prepared by reactions **5** and **6** have distinct patterns of fractional product yields (Table 4). The 1,3-dichloro-1-propen-2-yl radical ensembles prepared by reaction **6** produce substantial fractions of chloroallene and 1,2-dichloroallyl radical. The 2,3-dichloro-1-propen-1-yl radical ensembles produced by reaction **5** mainly undergo reverse reaction. The differences among the fractional product yields are symptomatic of the absence of steady-state kinetics during decomposition. In particular, the differing fractional product yields arise because reactions **7**, **−7** establish equilibrium between the incipient dichloro-vinyl isomers very slowly relative to the time scales of reactions **−5**, **−6**, **10**, **−10**, and **12**. (Discussions of the time evolution of non-steady-state systems are given in refs 11,12) In particular, the relatively high

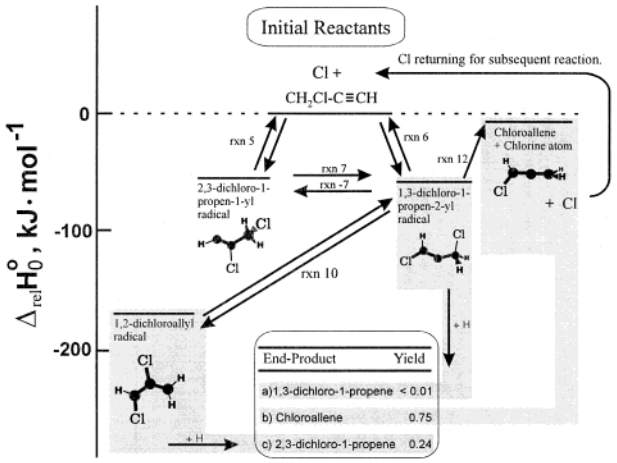

Figure 7. Kinetic reaction mechanism for Cl + propargyl chloride reaction comprised of the elementary processes that the ab initio calculations predict are exothermic relative to Cl + propargyl chloride. Shading reconciles each end-product observed with gas-chromatography with a reaction product channel. See text.

TS7 barrier largely isolates the chemically activated 2,3-dichloro-1-propen-1-yl ensemble from reactions **10** and **12**.

Validation of the reaction mechanism, derived from the ab initio results, is found in Table 4, by noting the accord of the predicted and measured the $\langle p_i \rangle$ at 298 K and 1010 Pa. Figure 7 outlines these experiments, where a static bulb containing a 1% propargyl chloride/99% helium molar mixture was exposed to 193 nm light, producing an ensemble of chlorine atoms that reacted with propargyl chloride. The stable reaction end-products were analyzed with gas chromatography and mass spectrometry (GC-MS).[8] Arrows indicate the active pathways of chlorine atom flux from initial reactants to products, including regeneration of chlorine atoms from $C_3H_3Cl_2$ ensembles through reactions **−5**, **−6**, and **12**. Figure 7 also shows bimolecular hydrogen abstraction steps that convert free radicals into the stable dichloro-1-propene isomers detected during GS-MS analyses.

(The figure does not depict secondary processes, such as collisional product stabilization in the bath and HCl metathesis reaction **3**.) The parent radical of each stable end-product is denoted with gray scale shading and the inset table lists the product abundances. According to diagram, the 2,3-dichloro-1-propene is mainly generated from the hydrogenation of the 1,2-dichloroallyl radicals and 1,3-dichloro-1-propene is formed through the hydrogenation of 1,3-dichloro-1-propen-2-yl radicals. Referenced to the chlorinated C3 product yield, the GC-MS analysis found chloroallene (0.75), 2,3-dichloro-1-propene (0.24), and 1,3-dichloro-1-propene (<0.01),[8] which are results in accord with the CHEMRATE predictions.

This validated model of the Cl + propargyl chloride reaction provides a good basis for estimating product distributions as a function of temperature and pressure. Although the present treatment is quantitative, the comparison between the end-product data and CHEMRATE results involves some necessary approximations. These approximations have little effect on the computed $\langle p_i \rangle$ and do not diminish the strength of this validation. First, the evaluation of eq 14 presumes, $k_5 \approx k_6$. The assumption is not supported by the radioactive labeling studies of Cl + propyne by Lee and Rowland who measured ^{38}Cl substituted products and concluded that chlorine adds to the end and center unsaturated carbons with an 8:1 ratio.[39] Nonetheless, for Cl + propargyl chloride such differences in relative reactivity for chlorine addition will have little effect because the $C_3H_3Cl_2$ ensemble produced by reaction **5** returns mainly to initial products, i.e., $f^5_{rev} \approx 0.9$, and the ensemble prepared by reaction **6** returns a much smaller fraction to initial reactants ($f^6_{rev} \approx 0.2$). As a result, the $\langle p_i \rangle$'s are more heavily weighted by the fractional product yields of reaction **6**. Second, although the experiment found a 3:1 ratio of chloroallene to 1,2-dichloro-1-propene, the measurements may have underestimated the contributions of reaction **10** if a significant fraction of the 1,2-dichloroallyl radical product was lost to recombination and cross-reaction before hydrogenation formed 2,3-dichloro-1-propene. Our CHEMRATE simulations indicate that small adjustments of $\Delta_f H_0^o$ (chloroallene) should easily accommodate future determinations of $\langle p_i \rangle$ for chloroallene and 1,2-dichloroallyl radical. During the CHEMRATE simulations we obtained the 3:1 ratio of chloroallene to 1,2-dichloro-1-propene with a 4 kJ·mol^{-1} increase in $\Delta_f H_0^o$ (chloroallene), which is within its uncertainty (Table 1). Without this increased $\Delta_f H_0^o$ (chloroallene) we obtained a 20:1 ratio. Finally, these calculations do not consider the effects of tunneling and internal rotors. When extensive data are available over an extended range of temperature and pressure, these effects can be added to the CHEMRATE model to improve fits of the observed falloff behavior and product distribution variation.

At 298 K and 1010 Pa the conversion yield per initial chlorine atom, $\langle C_i \rangle$, indicates that 97% of the initial chlorine concentration becomes sequestered in 1,2-dichloroallyl radical and $\approx$ 2% is sequestered by the HCl metathesis channel. In contrast, at 1000 K the calculations predict that $\approx$ 100% of the initial chlorine becomes sequestered in HCl metathesis product, even though the addition channels continue to dominate the Cl + propargyl reaction. The dominance of HCl metathesis over chlorine addition products at higher temperature is consistent with the report by Farrell and Taatjes who observed the metathesis reaction fraction of Cl + propyne to increase from 0.7 to 1.0 between 298 and 500 K.[36] Another feature of the Cl + propargyl chloride reaction, which is observed in $\langle C_i \rangle$, is the factor of 12 increase in chloroallene production between 298 and 1000 K (Table 4). In future experiments the chloroallene production may provide a clock for measuring relative rates across channels. In practical systems, such as incinerators, this process may play a catalytic route that isomerizes propargyl chloride into chloroallene.

Acknowledgment. We thank Dr. Jeffrey Manion for insightful discussions during the preparation of this manuscript. We also thank Dr. Wing Tsang and Dr. Donald Burgess for tutorials and help with the CHEMRATE calculations.

Supporting Information Available: Table 1S lists the $H^{Q(T)//QCISD}$ and $(H_0^{ZPE})^{MP2}$ for each persistent species. For each transition state, Table 2S lists the electronic energy, the zero point vibrational energy, and the fully optimized geometrical description with reference to the atom numbering system of Figure 1. Table 3S lists the input data for the CHEMRATE program. This material is available free of charge via the Internet at http://pubs.acs.org.

References and Notes

(1) Tsang, W. *Combust. Sci. and Technol.* **1990**, *74*, 99.
(2) *Chemical Kinetics Database on the Web, Standard Reference Database 17*, Version 7.0 (Web Version), Public Beta Release 1.0; National Institute of Standards and Technology, http://kinetics.nist.gov, 2001.
(3) Hudgens, J. W.; Gonzalez, C. *J. Chem. Phys. A* **2002**, *106*, 1739.
(4) Atkinson, D. B.; Hudgens, J. W. *J. Phys. Chem. A* **2000**, *104*, 811−818.
(5) Atkinson, D. B.; Hudgens, J. W. *J. Phys. Chem. A* **1999**, *103*, 4242.
(6) Morter, C. L.; Farhat, S. K.; Adamson, J. D.; Glass, G. P.; Curl, R. F. *J. Phys. Chem.* **1994**, *98*, 7029.
(7) Fahr, A.; Nayak, A. *Internat. J. Chem. Kinet.* **2000**, *32*, 118−124.
(8) Atkinson, D. B.; Hudgens, J. W. *J. Phys. Chem.* **1999**, *103*, 7978−7989.
(9) *ChemRate: A Calculational Data Base for Unimolecular Reaction*, ver. 1.19; Mokrushin, V., Bedanov, V., Tsang, W., Zachariah, M., Knyazev, V.; National Institute of Standards and Technology Gaithersburg, MD 20899, U.S.A., http://www.nist.gov/kinetics/Chemrate/chemrate.html, 2002.
(10) Tsang, W. "A Preprocessor for the Generation of Chemical Kinetics Data for Simulations"; 39th AIAA Aerospace Sciences Meeting and Exhibit, Jamuary 8−11, 2001 Reno. NV, 2001, Reno. NV.
(11) Tsang, W.; Bedanov, V.; Zachariah, M. R. *Berichte Der Bunsen-Gesellschaft-Physical Chemistry Chemical Physics* **1997**, *101*, 491.
(12) Tsang, W.; Bedanov, V.; Zachariah, M. R. *J. Phys. Chem.* **1996**, *100*, 4011−4018.
(13) Certain commercial materials and equipment are identified in this paper in order to adequately specify the experimental procedure. Such identification neither implies recommendation or endorsement by the National Institute of Standards and Technology, nor does it imply that the material or equipment identified is the best available for the purpose.
(14) Frisch, M. J.; Trucks, G. W.; Schlegel, H. B.; Scuseria, G. E.; Robb, M. A.; Cheeseman, J. R.; Zakrzewski, V. G.; Montgomery, J. A., Jr.; Stratmann, R. E.; Burant, J. C.; Dapprich, S.; Millam, J. M.; Barone, V.; Cossi, M.; Cammi, R.; Mennucci, B.; Pomelli, C.; Adamo, C.; Clifford, S.; Ochterski, J.; Petersson, G. A.; Ayala, P. Y.; Cui, Q.; Morokuma, K.; Malick, D. K.; Rabuck, A. D.; Raghavachari, K.; Foresman, J. B.; Cioslowski, J.; Ortiz, J. V.; Baboul, A. G.; Stefanov, B. B.; Liu, G.; Liashenko, A.; Piskorz, P.; Komaromi, I.; Gomperts, R.; Martin, R. L.; Fox, D. J.; Keith, T.; Al-Laham, M. A.; Peng, C. Y.; Nanayakkara, A., Gonzalez, C.; Challacombe, M.; Gill, P. M. W.; Johnson, B.; Chen, W.; Wong, M. W.; Andres, J. L.; Head-Gordon, M.; Replogle, E. S.; Pople, J. A. *Gaussian 98*, revision A.7; Gaussian, Inc., Pittsburgh, PA, 1998.
(15) Frisch, M. J.; Trucks, G. W.; Schlegel, H. B.; Gill, P. M. W.; Johnson, B. G.; Robb, M. A.; Cheeseman, J. R.; Keith, T.; Petersson, G. A.; Montgomery, J. A.; Raghavachari, K.; Al-Laham, M. A.; Zakrzewski, V. G.; Ortiz, J. V.; Foresman, J. B.; Cioslowski, J.; Stefanov, B. B.; Nanayakkara, A.; Challacombe, M.; Peng, C. Y.; Ayala, P. Y.; Chen, W.; Wong, M. W.; Andres, J. L.; Replogle, E. S.; Gomperts, R.; Martin, R. L.; Fox, D. J.; Binkley, J. S.; Defrees, D. J.; Baker, J.; Stewart, J. P.; Head-Gordon, M.; Gonzalez, C.; Pople, J. A. *Gaussian 94*, revision D.4; Gaussian, Inc.: Pittsburgh, PA, 1995.
(16) Møller, C.; Plesset, M. S. *Phys. Rev.* **1968**, *46*, 4852.
(17) Becke, A. D. *J. Chem. Phys* **1993**, *98*, 5648.
(18) Pople, J. A.; Head-Gordon, M.; Raghavachari, K. *J. Chem. Phys.* **1987**, *87*, 5968.
(19) Hehre, W. J.; Ditchfield, R.; Pople, J. A. *J. Chem. Phys.* **1972**, *56*, 2257.
(20) Hariharan, P. C.; Pople, J. A. *Theo. Chim. Acta* **1973**, *28*, 213.

(21) Frisch, M. J.; Pople, J. A.; Binkley, J. S. *J. Chem. Phys.* **1984**, *80*, 3265.
(22) Ditchfield, R.; Hehre, W. J.; Pople, J. A. *J. Chem. Phys.* **1971**, *54*, 724.
(23) Clark, T.; Chandrasekhar, J.; Spitznagel, G. W.; Schleyer, P. V. R. *J. Comp, Chem.* **1983**, *4*, 294.
(24) Schlegel, H. B. *J. Phys. Chem.* **1988**, *92*, 3075.
(25) Schlegel, H. B. *J. Chem. Phys.* **1986**, *84*, 4530.
(26) Sosa, C.; Schlegel, H. B. *Int. J. Quantum Chem.* **1986**, *29*, 1001.
(27) Sosa, C.; Schlegel, H. B. *Int. J. Quantum Chem.* **1987**, *30*, 155.
(28) Gonzalez, C.; Schlegel, H. B. *J. Chem. Phys.* **1991**, *95*, 5853.
(29) Gonzalez, C.; Schlegel, H. B. *J. Chem. Phys.* **1989**, *90*, 2154.
(30) Gonzalez, C.; Schlegel, H. B. *J. Phys. Chem.* **1990**, *94*, 5523.
(31) *NIST Computational Chemistry Comparison and Benchmark DataBase version 5*, Release 5b; Johnson, R. D., III, *http://srdata.nist.gov/cccbdb*, Oct 2001.
(32) The scaling factors were derived using the experimentally measured vibrational frequencies of chloroethene, chloroform, ethyl chloride, methyl chloride, methylene chloride, 1,2-dichloro-ethane, (E)-1,2-dichloro-ethene, (Z)-1,2-dichloro-ethene, and 2-chloro-propane.
(33) Eyring, H. J. *J. Chem. Phys.* **1935**, *3*, 107.
(34) Glasstone, S.; Laidler, K. J.; Eyring, H. *The Theory of Rate Processes*; McGraw-Hill: New York, 1941.
(35) Steinfeld, J. I.; Francisco, J. S.; Hase, W. L. *Chemical Kinetics and Dynamics*; Prentice Hall: New Jersey, 1989.
(36) Farrell, J. T.; Taatjes, C. A. *J. Phys. Chem. A* **1998**, *102*, 4846.
(37) Wallington, T. J.; Skewes, L. M.; Siegl, W. O. *J. Photochem. Photobiol. A. Chem.* **1988**, *45*, 167.
(38) Bartlett, R. D. Chapter 16. In *Modern Electronic Structure Theory Part II*; Yarkony, D. R., Ed.; World Scientific: Singapore, 1995; Vol. 2.
(39) Lee, F. S. C.; Rowland, F. S. *J. Phys. Chem.* **1980**, *84*, 1876−1881.
(40) Tschuikow-Roux, E.; Niedzielski, J.; Faraji, F. *Can. J. Chem.* **1985**, *63*, 1093.
(41) Pontsma, M. L. *J. Am. Chem. Soc.* **1965**, *87*, 2172.
(42) Fahr, A.; Hassanzadeh, P.; Laszlo, B.; Huie, R. E. *Chem. Phys.* **1997**, *215*, 59.
(43) Gilbert, R. G.; Smith, S. C. *Theory of Unimolecular and Recombination Reactions*; Blackwell Scientific Publications: Oxford, 1990.
(44) Tsang, W.; Kiefer, J. R. Unimolecular Reactions of Large Polyatomic Molecules over Wide Temperature Ranges. In *The Chemical Dynamics and Kinetics of Small Radicals, Part I*; Liu, K., Wagner, A., Eds.; World Scientific: Singapore, 1995; p 58.
(45) Chase, M. W., Jr.; Davies, C. A.; Downey, J. R., Jr.; Frurip, D. J.; McDonald, R. A.; Syverud, A. N. *J. Phys. Chem. Ref. Data* **1985**, *14*.
(46) Tsang, W. Heats of Formation of Organic Free Radicals by Kinetic Methods in Energetics of Organic Free Radicals. In *Energetics of Organic Free Radicals*; Simoes, J. A., Greenberg, A., Liebman, J. F., Eds.; Blackie Academic and Professional: London, 1996; pp 22−58.